

# Quantum Paramagnet and Frustrated Quantum Criticality in a Spin-One Diamond Lattice Antiferromagnet

Gang Chen<sup>1,2\*</sup>

<sup>1</sup>State Key Laboratory of Surface Physics, Department of Physics, Center for Field Theory & Particle Physics, Fudan University, Shanghai, 200433, China and

<sup>2</sup>Collaborative Innovation Center of Advanced Microstructures, Nanjing, 210093, China

(Dated: February 20, 2022)

Motivated by the proposal of *topological quantum paramagnet* in the diamond lattice antiferromagnet  $\text{NiRh}_2\text{O}_4$ , we propose a minimal model to describe the magnetic interaction and properties of the diamond material with the spin-one local moments. Our model includes the first and second neighbor Heisenberg interactions as well as a local single-ion spin anisotropy that is allowed by the spin-one nature of the local moment and the tetragonal symmetry of the system. We point out that there exists a quantum phase transition from a *trivial quantum paramagnet* when the single-ion spin anisotropy is dominant to the magnetic ordered states when the exchange is dominant. Due to the frustrated spin interaction, the magnetic excitation in the quantum paramagnetic state supports *extensively degenerate band minima* in the spectra. As the system approaches the transition, extensively degenerate bosonic modes become critical at the criticality, giving rise to unusual magnetic properties. Our phase diagram and experimental predictions for different phases provide a guideline for the identification of the ground state for  $\text{NiRh}_2\text{O}_4$ . Although our results are fundamentally different from the proposal of topological quantum paramagnet, it represents interesting possibilities for spin-one diamond lattice antiferromagnets.

*Introduction.*—The recent theoretical proposal of symmetry protected topological (SPT) ordered states has sparked a wide interest in the theoretical community<sup>1–25</sup>. The well-known topological insulator, that was proposed and discovered earlier, is a *non-interacting* fermion SPT protected by time reversal symmetry<sup>26,27</sup>. In contrast, the SPTs in bosonic systems must be stabilized by the interactions<sup>11</sup>. The spin degrees of freedom with exchange interactions seem to be a natural candidate for realizing the boson SPTs<sup>10</sup>. In fact, the Haldane spin-one chain is a 1D boson SPT and is protected by the  $\text{SO}(3)$  spin rotational symmetry<sup>1,2,28</sup>. The realization of boson SPTs in high dimensions is still missing. It was suggested that, the spin-one diamond lattice antiferromagnet with frustrated spin interactions may host a topological quantum paramagnet that is a spin analogue of topological insulator and protected by time reversal symmetry<sup>29</sup>. Quite recently, a diamond lattice antiferromagnet  $\text{NiRh}_2\text{O}_4$  with  $\text{Ni}^{2+}$  spin-one local moments was proposed to fit into the early suggestion<sup>30</sup>.

$\text{NiRh}_2\text{O}_4$  is a tetragonal spinel and experiences a structural phase transition from cubic to tetragonal at  $T = 380\text{K}$ <sup>30,32,33</sup>. As we show in Fig. 1, the magnetic ion  $\text{Ni}^{2+}$  has a  $3d^8$  electron configuration, forming a spin  $S = 1$  local moment and occupying the tetrahedral diamond lattice site. No signature of magnetic order was observed down to 0.1K in the magnetic susceptibility and specific heat measurements. Although this might fulfill the basic requirement of the absence of magnetic order in a topological quantum paramagnet, alternative state, that is distinct from topological quantum paramagnet, may also provide a consistent experimental prediction with the current experiments. In this Rapid Communication, we propose a minimal spin model for spin-one diamond lattice with tetragonal distortion and study the

full phase diagram and the phase transition of our model. We do not find the presence of the topological quantum paramagnet in our phase diagram. Instead, due to the strong spin frustration, the ordered state in our phase diagram can be easily destabilized and converted into a trivial quantum paramagnet by a moderate single-ion spin anisotropy. We predict that this seemingly trivial quantum paramagnetic state in a large parameter regime supports gapped magnetic excitation that develops *extensively degenerate band minima* in the spectrum. As the quantum paramagnet approaches the phase transition to the proximate ordered state, the extensively degenerate low-energy modes become gapless and are re-

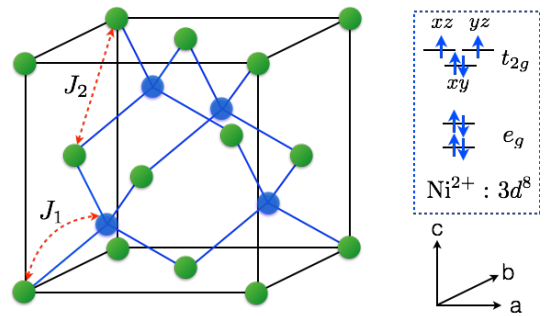


FIG. 1. (Color online.) The diamond lattice with the  $J_1$  and  $J_2$  interactions. Due to the tetragonal symmetry of the lattice, the  $a$  and  $b$  directions are not equivalent to the  $c$  direction. The  $\text{Ni}^{2+}$  ion is in a tetrahedral environment, so the  $e_g$  orbitals are lower in energy than the  $t_{2g}$  levels. The tetragonal distortion further splits the two  $e_g$  orbitals and the three  $t_{2g}$  orbitals. But the degeneracy of the  $xz$  and  $yz$  orbitals remains intact under the tetragonal distortion. To avoid the orbital degree of freedom, we here place the  $xz$  and  $yz$  orbitals above the  $xy$  orbitals<sup>31</sup>.

sponsible for the unusual magnetic properties such as the *linear-T heat capacity* at low temperatures in the vicinity of the transition. In the proximate ordered phases, we further show that the spin spiral orders are actually induced by quantum fluctuations via quantum order by disorder.

*The microscopic spin model.*—We here propose the following microscopic spin model that describes the interaction between the spin-1 local moments with the tetragonal symmetry,

$$H = J_1 \sum_{\langle rr' \rangle} \mathbf{S}_r \cdot \mathbf{S}_{r'} + J_2 \sum_{\langle\langle rr' \rangle\rangle} \mathbf{S}_r \cdot \mathbf{S}_{r'} + D_z \sum_r (S_r^z)^2, \quad (1)$$

where  $J_1$  and  $J_2$  are the first neighbor and second neighbor Heisenberg exchange interactions, respectively. Although the tetragonal lattice symmetry allows inequivalent bonds<sup>33</sup>, in this minimal model we assume all the bonds are equivalent. Since the diamond lattice is a bipartite lattice, the first neighbor  $J_1$  interaction alone is unfrustrated, and would favor a simple Néel state if  $J_1$  is antiferromagnetic. The second neighbor interaction  $J_2$  is an interaction within each FCC sublattice of the diamond lattice. Due to the large numbers of second neighbor bonds, the  $J_2$  interaction would cause a spin frustration even when it is small compared to  $J_1$ . Moreover, an additional single-ion spin anisotropy is further introduced on top of the spin exchange interactions, and is not included in the model in Ref. 33. The spin anisotropy is naturally allowed by the tetragonal lattice symmetry and is the only term occurring for a spin-one local moment like the  $\text{Ni}^{2+}$  ion. Previous classical treatment of the  $J_1$ - $J_2$  spin model on a diamond lattice and the analysis of thermal fluctuation have led to the interesting discovery of the spiral spin liquid<sup>34-37</sup>. A quantum treatment of  $J_1$ - $J_2$  model used an exotic SP(N) parton construction for the spins<sup>38</sup> and again worked in the ordered regime. In our context, we will largely treat spins and interactions quantum mechanically with a more conventional means that is appropriate for the  $J_1$ - $J_2$ - $D_z$  model.

Due to this single-ion spin anisotropy, the magnetic susceptibilities along different directions should reveal such spin anisotropy. In particular, we carry out the high temperature series expansion and find that the Curie-Weiss temperatures for the magnetic field parallel and normal to the  $z$  direction are given as<sup>31</sup>

$$\Theta_{\text{CW}}^z = -\frac{D_z}{3} - \frac{S(S+1)}{3}(z_1 J_1 + z_2 J_2), \quad (2)$$

$$\Theta_{\text{CW}}^\perp = +\frac{D_z}{6} - \frac{S(S+1)}{3}(z_1 J_1 + z_2 J_2), \quad (3)$$

where  $z_1 = 4$  and  $z_2 = 12$  are the numbers of first neighbor and second neighbor bonds, respectively. The above prediction can be used to extract the single-ion spin anisotropy. Note for a powder sample, the Curie-Weiss temperature is  $\Theta_{\text{CW}}^{\text{Powder}} = -\frac{S(S+1)}{3}(z_1 J_1 + z_2 J_2)$  and is thus independent of the spin anisotropy.

*Quantum paramagnet and phase diagram.*—To obtain the full phase diagram of the  $J_1$ - $J_2$ - $D_z$  model, we

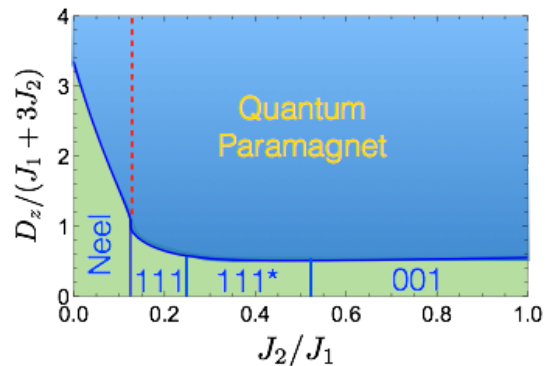


FIG. 2. (Color online.) The phase diagram of the  $J_1$ - $J_2$ - $D_z$  model. Because the powder sample Curie-Weiss temperature  $\Theta_{\text{CW}}^{\text{Powder}} = -8(J_1 + 3J_2)/3$ , we set the energy unit of the spin anisotropy  $D_z$  to  $J_1 + 3J_2$  in the plot. The transition from the quantum paramagnet to the ordered regions is continuous at the mean-field theory. On the left of the (red) dashed line, the band minimum of the magnetic excitation is unique and appears at  $\Gamma$  point. On the right side, the band minima form a degenerate surface in the reciprocal space. Please refer the main text for details.

start from the parameter regime where the single-ion spin anisotropy is dominant. We consider the easy-plane anisotropy with  $D_z > 0$ , since the easy-axis spin anisotropy would stabilize the Néel state and enlarge its parameter regime. In the large and positive  $D_z$  limit, the ground state is a trivial quantum paramagnet with  $S^z = 0$  on every site,  $|\Psi\rangle = \prod_r |S_r^z = 0\rangle$ . For this simple state, there is no magnetic order and all the spin excitations are fully gapped. Since the global  $U(1)$  spin rotational symmetry around the  $z$  direction is preserved, the magnetic susceptibility at zero temperature for the field along the  $z$  direction is zero with  $\chi_z(T=0) = 0$ . However, if the field is applied in the  $xy$  plane, the spin rotational symmetry is broken by the in-plane field and the magnetic susceptibility is a constant with

$$\chi_\perp(T=0) = \frac{2\mu_0(g\mu_B)^2}{D_z + 2(z_1 J_1 + z_2 J_2)}, \quad (4)$$

where  $g$  is the Lande factor. Again, this result is a consequence of the single-ion anisotropy and can be used to detect the quantum paramagnetic state.

As we turn on the exchange interaction, the spin excitation would develop dispersion in the momentum space. With a sufficient exchange interaction, we expect the minimum of the dispersion to touch the zero energy that would lead to magnetic orderings. To describe the magnetic ordering transition out of the quantum paramagnetic phase, we substitute the spin operators with the rotor variables such that<sup>39</sup>

$$S_r^z = n_r, \quad S_r^\pm = \sqrt{2}e^{\pm i\phi_r}, \quad (5)$$

where  $\phi_r$  is a  $2\pi$ -periodic phase variable and  $n_r$  is integer-valued. This substitution has enlarged the physical Hilbert space by allowing  $S^z$  or  $n$  to take the values

beyond 0 and  $\pm 1$ . We, however, do not expect this approximation to cause significant effects since the non-physical values of  $n_r$  has been energetically suppressed by the large single-ion spin anisotropy. Moreover, the substitution preserves the global U(1) spin rotational symmetry around the  $z$  direction of the original spin model. Finally, to preserve the spin commutation relation, we impose the commutation for  $\phi_r$  and  $n_r$  with  $[\phi_r, n_{r'}] = i\delta_{rr'}$ .

With the rotor variables, the  $J_1$ - $J_2$ - $D_z$  spin model takes the form

$$\begin{aligned}
H = & \sum_{\langle rr' \rangle} J_1 [2 \cos(\phi_r - \phi_{r'}) + n_r n_{r'}] \\
& + \sum_{\langle\langle rr' \rangle\rangle} J_2 [2 \cos(\phi_r - \phi_{r'}) + n_r n_{r'}] \\
& + \sum_r D_z n_r^2.
\end{aligned} \tag{6}$$

From the symmetry point of view, the above model has the same symmetry as a standard boson Hubbard model except having an extra inter-site boson interaction. To make this analogy a bit further, the quantum paramagnetic state is analogous to a boson Mott insulator with  $n_r = 0$  at every site, and the proximate magnetic order is like a superfluid of bosons. Despite the seemingly similarity, we show below the intrinsic spin frustration brings rather interesting dispersion of magnetic excitation in the quantum paramagnet and thus leads to unusual properties at the analogous ‘‘superfluid-Mott’’ transition<sup>40</sup>.

The primary operators that are responsible for the magnetic transition out of the quantum paramagnet are the  $S_r^\pm$  spin operators that create the gapped spin excitations in the quantum paramagnet but take finite values in the ordered states. We here carry out the coherent state path integral and integrate out the number operator  $n_r$ . The resulting partition function is

$$Z = \int \mathcal{D}\Phi_r \mathcal{D}\lambda_r \exp[-S - \mathfrak{i} \sum_r \lambda_r (|\Phi_r|^2 - 1)], \tag{7}$$

where the effective action for the rotor variable is

$$\begin{aligned}
S = & \int d\tau \sum_{\mathbf{k} \in \text{BZ}} (2D_z \mathbb{1}_{2 \times 2} + \mathcal{J}_{\mathbf{k}})^{-1} \partial_\tau \Phi_{i,\mathbf{k}}^\dagger \partial_\tau \Phi_{j,\mathbf{k}} \\
& + \sum_{\langle rr' \rangle} J_1 \Phi_r^\dagger \Phi_{r'} + \sum_{\langle\langle rr' \rangle\rangle} J_2 \Phi_r^\dagger \Phi_{r'},
\end{aligned} \tag{8}$$

where we have introduced the variable  $\Phi_r \equiv e^{i\phi_r}$ . To impose the unimodular condition for  $\Phi_r$ , we have introduced a Lagrange multiplier  $\lambda_r$  on each site to impose the unimodular condition  $|\Phi_r| = 1$  in Eq. (7). To solve for the dispersion of the excitation, we take a saddle point approximation and choose a uniform mean-field ansatz such that  $\mathfrak{i}\lambda_r \equiv \beta\Delta(T)$  where  $\beta = (k_B T)^{-1}$ . We integrate out the  $\Phi_r$  field and obtain the saddle-point equation for  $\Delta(T)$  in the quantum paramagnetic phase

$$\sum_{i=1,2} \sum_{\mathbf{k} \in \text{BZ}} \frac{2D_z + \xi_{i,\mathbf{k}}}{\omega_{i,\mathbf{k}}} \coth\left(\frac{\beta\omega_{i,\mathbf{k}}}{2}\right) = 2, \tag{9}$$

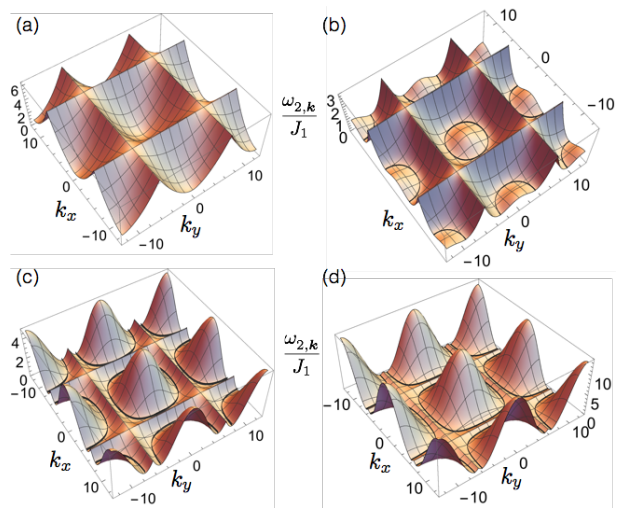


FIG. 3. (Color online.) The magnetic excitation  $\omega_{2,\mathbf{k}}$  in the  $k_x$ - $k_y$  plane of the quantum paramagnet. We have chosen the following parameters (a)  $J_2 = 0.05J_1, D_z = 3J_1$ ; (b)  $J_2 = 0.18J_1, D_z = 1.5J_1$ ; (c)  $J_2 = 0.4J_1, D_z = 1.5J_1$ ; (d)  $J_2 = 0.8J_1, D_z = 2J_1$ . In the figure, we set  $k_z = 0$ , and an extended zone with  $k_x \in [-4\pi, 4\pi], k_y \in [-4\pi, 4\pi]$  is used. The degenerate minima are marked with contours. One can observe the evolution of the band minima.

where  $\omega_{1,\mathbf{k}}$  and  $\omega_{2,\mathbf{k}}$  are the two modes of the magnetic excitations in the paramagnetic phase and are given by

$$\omega_{i,\mathbf{k}} = [(4D_z + 2\xi_{i,\mathbf{k}})(\Delta(T) + \xi_{i,\mathbf{k}})]^{\frac{1}{2}}, \tag{10}$$

and  $\xi_{1,\mathbf{k}}$  and  $\xi_{2,\mathbf{k}}$  are the two eigenvalues of the exchange matrix  $\mathcal{J}_{\mathbf{k}}$ <sup>31</sup>. As one decreases the single-ion spin anisotropy, the gap of the magnetic excitation decreases steadily. At the transition, the gap is closed and induces the magnetic order, and this phase transition is continuous within this treatment. In the phase diagram that is depicted in Fig. 2, the phase boundary between the quantum paramagnet and the magnetic order is then determined by examining the gap of the excitations in Eq. (10). In Fig. 2, the ordered region of the phase diagram is further splitted into several sub-regions with distinct magnetic orders from the quantum order by disorder effect. This will be explained below soon.

*Frustrated quantum criticality.*—Here we point out the nontrivial magnetic excitation in the quantum paramagnetic state and the resulting frustrated quantum criticality. When  $J_2 < J_1/8$ , the band minimum of the lower excitation  $\omega_{2,\mathbf{k}}$  is at the  $\Gamma$  point. As we increase  $J_2$  beyond  $J_1/8$ , the dispersion minima are obtained by minimizing  $\xi_{2,\mathbf{k}}$ . We find that the minima of  $\omega_{2,\mathbf{k}}$  are extensively degenerate<sup>41,42</sup> and form a two-dimensional surface in the three-dimensional reciprocal space that is defined by

$$\cos \frac{k_x}{2} \cos \frac{k_y}{2} + \cos \frac{k_x}{2} \cos \frac{k_z}{2} + \cos \frac{k_y}{2} \cos \frac{k_z}{2} = \frac{J_1^2}{16J_2^2} - 1, \tag{11}$$

where we have set the lattice constant to unity. This relation coincides with the degenerate spiral surface that

was obtained in the classical treatment of the  $J_1$ - $J_2$  model<sup>34,43</sup>. In Fig. 3, we depict the band  $\omega_{2,\mathbf{k}}$  in the  $k_x$ - $k_y$  plane with  $k_z = 0$ .

Now we explain how the behavior of the heat capacity in the vicinity of the magnetic critical point are modified by the large density of the low-energy excitations near the band minima. For  $J_2 < J_1/8$ , only a single bosonic mode becomes critical (see Fig. 3a) and leads to the usual  $C_v \propto T^3$  up to a logarithmic correction from the quantum fluctuation at the criticality. For  $J_2 > J_1/8$ , however, a *degenerate surface of bosonic modes* become critical at the transition (see Fig. 3b,c,d). To understand the consequence of this unusual phenomena, we return to the saddle point equation in Eq. (9) that reduces to

$$A \int_0^\Lambda dk_\perp \int_\Sigma d^2 \mathbf{k}_t \frac{\coth[\frac{\beta}{2}(m^2 + v^2 k_\perp^2)^{\frac{1}{2}}]}{(m^2 + v^2 k_\perp^2)^{\frac{1}{2}}} + c = 2, \quad (12)$$

where we have singled out the contribution from the critical modes as the first term in Eq. (12),  $A$  is an unimportant prefactor of the integration, and  $c$  is approximately  $T$ -independent contribution from the remaining part of the excitations. In Eq. (12), we have chosen the coordinate basis  $(\mathbf{k}_t, k_\perp)$  such that  $\mathbf{k}_t$  ( $k_\perp$ ) refer to the components of the momentum tangential to (normal to) the degenerate surface  $\Sigma$  (see Fig. 4), and  $\Lambda$  is the momentum cutoff. Here the critical mode behaves  $\omega_{2,\mathbf{k}} \simeq (m^2 + v^2 k_\perp^2)^{\frac{1}{2}}$  in which  $m$  is the thermally generated mass term and  $v$  is the velocity normal to the degenerate surface. At low temperatures ( $T \ll \Lambda$ ), the temperature dependent part of the integral becomes independent of the cutoff  $\Lambda$ , and only depends on  $T$  via the dimensionless parameter  $m^2/T^2$ . In order for the equality in Eq. (12) to hold, we expect  $m \propto T$ .

From the scaling form of  $m$ , we obtain a remarkable result for the low-temperature heat capacity that behaves as  $C_v \propto T$  at the criticality. This linear- $T$  heat capacity is like the one in a Fermi liquid metal, except that this is a pure bosonic system! This unusual behavior simply arises from the frustrated spin interaction.

*Quantum order by disorder.*—When the extensively degenerate modes are condensed at the critical point for  $J_2 > J_1/8$ , extensively degenerate candidate ordered states are available, and it is the quantum fluctuation of the spins that selects the the particular orders in the phase diagram of Fig. 2.

To explain this phenomenon, we first realize that the easy-plane spin anisotropy favors the magnetic order in the  $xy$  plane with

$$\mathbf{r} \in \text{A}, \quad \mathbf{S}_\mathbf{r} = S \text{Re}[(\hat{x} - i\hat{y})e^{i\mathbf{q}\cdot\mathbf{r}}], \quad (13)$$

$$\mathbf{r} \in \text{B}, \quad \mathbf{S}_\mathbf{r} = S \text{Re}[(\hat{x} - i\hat{y})e^{i\mathbf{q}\cdot\mathbf{r} + i\theta_\mathbf{q}}], \quad (14)$$

where  $\mathbf{q}$  is the propagating wavevector of the spin spiral, and  $\theta_\mathbf{q}$  is the phase shift between A and B sublattices of the diamond lattice. Both  $\mathbf{q}$  and  $\theta_\mathbf{q}$  can be obtained by a Weiss mean-field theory that is like the early classical treatment<sup>34</sup>. The quantum fluctuation with respect to the candidate spin spiral state is analyzed by a linear spin-wave theory and is discussed in the detail in the

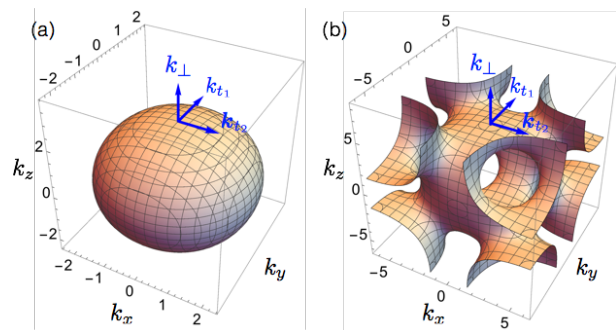


FIG. 4. (Color online.) The degenerate surface of the band minima at (a)  $J_2 = 0.18J_1$  and (b)  $J_2 = J_1/3$ . The  $(k_{t_1}, k_{t_2})$  are the two tangential momenta and  $k_\perp$  is the component normal to the degenerate surface.

Supplementary information. As we plot in Fig. 2, quantum fluctuation favors the spiral wavevector to be either along [001] or [111] direction. For  $J_2 > J_1/4$ , the degenerate surface has expanded to the Brillouin zone boundary, and the [111] direction no longer intersects with the degenerate surface (see Fig. 4b as an example), the six points around the [111] direction are selected, and the resulting ordering states are labeled by [111\*] in Fig. 2.

*Discussion.*—In contrary to the proposal of a topological quantum paramagnet in  $\text{NiRh}_2\text{O}_4$ <sup>30</sup>, our theoretical prediction does not support topological quantum paramagnet in our minimal  $J_1$ - $J_2$ - $D_z$  spin model. Instead, due to the strong frustrated spin interaction, a large region of trivial quantum paramagnet state is stabilized in the phase diagram. Although the trivial quantum paramagnet does not represent any new state of matter, the magnetic excitation is rather unusual and supports a degenerate surface of band minima in the spectrum. As the system is driven into a magnetic ordered state, extensively degenerate critical modes from the degenerate surface are condensed, leading to an unconventional critical properties at the transition.

To differentiate the proposal of topological quantum paramagnet and our proposal, we propose the following experiments. In a topological quantum paramagnet, the bulk is fully gapped and the surface may show various anomalous behaviors<sup>7,11,23,29</sup>. If the system develops gapless surface states, it should be detectable by the surface thermal transport. If the system realizes intrinsic topological order<sup>7,23</sup>, one would observe fractionalized excitations on the surface. If the system breaks the time reversal symmetry on the surface, then one would observe a surface magnetic order. In contrast, our prediction of the thermodynamic properties and the excitation spectrum for the trivial quantum paramagnet can be directly measured by the bulk measurements such as magnetic susceptibility and inelastic neutron scattering. Moreover, since the model is applicable broadly to spin-one tetragonal diamond materials, it is of interest to find similar materials in the spinel families.

Finally, we address the role of other interactions. It

has been shown *classically* for the spin  $S = 5/2$  diamond lattice antiferromagnet  $\text{MnSc}_2\text{S}_4$  that very weak third neighbor interaction could lift the continuous degeneracy<sup>34</sup>. Here, the quantum paramagnetic phase is a robust state, the presence of weak further neighbor interaction cannot destabilize it and we expect the general structure of the phase diagram in Fig. 2 to stay intact. The effect of the other weak interactions on the excitation in quantum paramagnet is a very low energy scale property and may not be visible under the current experimental resolution.

*Acknowledgements.*—We acknowledge one anonymous referee for criticism and comment that helps improve the paper. This work is supported by the Ministry of Science and Technology of China with the Grant No.2016YFA0301001, the Start-Up Funds and the Program of First-Class University Construction of Fudan

University, and the Thousand-Youth-Talent Program of China. We thank Prof Nanlin Wang for the hospitality during my visit at ICQM of Peking University, Prof Zhong Wang for the hospitality during my visit at IAS of Tsinghua University, Prof Chen Fang for the hospitality during my visit at IOP, and Prof Ying Ran for the hospitality during my visit at Boston College this January when this work was motivated and finalized. We thank Prof Yang Qi and Dr. Peng Ye for a Wechat conversation that points other surface possibilities that are consistent with Prof Senthil’s later comments. Finally, we thank Prof McQueen and Prof Senthil for the recent correspondence and comments. *Notes added:* During the review process of our work, a preprint<sup>44</sup> appeared and studied a modified exchange model for  $\text{NiRh}_2\text{O}_4$ . Their results are complementary to ours.

- 
- \* [gangchen.physics@gmail.com](mailto:gangchen.physics@gmail.com)
- <sup>1</sup> Zheng-Cheng Gu and Xiao-Gang Wen, “Tensor-entanglement-filtering renormalization approach and symmetry-protected topological order,” *Phys. Rev. B* **80**, 155131 (2009).
  - <sup>2</sup> Frank Pollmann, Ari M. Turner, Erez Berg, and Masaki Oshikawa, “Entanglement spectrum of a topological phase in one dimension,” *Phys. Rev. B* **81**, 064439 (2010).
  - <sup>3</sup> Xie Chen, Zheng-Cheng Gu, and Xiao-Gang Wen, “Classification of gapped symmetric phases in one-dimensional spin systems,” *Phys. Rev. B* **83**, 035107 (2011).
  - <sup>4</sup> Frank Pollmann, Erez Berg, Ari M. Turner, and Masaki Oshikawa, “Symmetry protection of topological phases in one-dimensional quantum spin systems,” *Phys. Rev. B* **85**, 075125 (2012).
  - <sup>5</sup> Xie Chen, Zheng-Cheng Gu, Zheng-Xin Liu, and Xiao-Gang Wen, “Symmetry protected topological orders and the group cohomology of their symmetry group,” *Phys. Rev. B* **87**, 155114 (2013).
  - <sup>6</sup> T Senthil, “Symmetry-protected topological phases of quantum matter,” *Annu. Rev. Condens. Matter Phys.* **6**, 299–324 (2015).
  - <sup>7</sup> Ashvin Vishwanath and T. Senthil, “Physics of Three-Dimensional Bosonic Topological Insulators: Surface-Deconfined Criticality and Quantized Magnetoelectric Effect,” *Phys. Rev. X* **3**, 011016 (2013).
  - <sup>8</sup> Cenke Xu and T. Senthil, “Wave functions of bosonic symmetry protected topological phases,” *Phys. Rev. B* **87**, 174412 (2013).
  - <sup>9</sup> Chong Wang and T. Senthil, “Boson topological insulators: A window into highly entangled quantum phases,” *Phys. Rev. B* **87**, 235122 (2013).
  - <sup>10</sup> Xie Chen, Zheng-Cheng Gu, and Xiao-Gang Wen, “Complete classification of one-dimensional gapped quantum phases in interacting spin systems,” *Phys. Rev. B* **84**, 235128 (2011).
  - <sup>11</sup> Xie Chen, Zheng-Cheng Gu, Zheng-Xin Liu, and Xiao-Gang Wen, “Symmetry-protected topological orders in interacting bosonic systems,” *Science* **338**, 1604–1606 (2012).
  - <sup>12</sup> Hao Song, Sheng-Jie Huang, Liang Fu, and Michael Hermele, “Topological phases protected by point group symmetry,” arXiv preprint arXiv:1604.08151 (2016).
  - <sup>13</sup> Max A. Metlitski, C. L. Kane, and Matthew P. A. Fisher, “Bosonic topological insulator in three dimensions and the statistical Witten effect,” *Phys. Rev. B* **88**, 035131 (2013).
  - <sup>14</sup> Max A. Metlitski, C. L. Kane, and Matthew P. A. Fisher, “Symmetry-respecting topologically ordered surface phase of three-dimensional electron topological insulators,” *Phys. Rev. B* **92**, 125111 (2015).
  - <sup>15</sup> Yuan-Ming Lu and Ashvin Vishwanath, “Theory and classification of interacting integer topological phases in two dimensions: A chern-simons approach,” *Phys. Rev. B* **86**, 125119 (2012).
  - <sup>16</sup> Xie Chen, Yuan-Ming Lu, and Ashvin Vishwanath, “Symmetry-protected topological phases from decorated domain walls,” *Nature communications* **5** (2014).
  - <sup>17</sup> Zhen Bi, Alex Rasmussen, Kevin Slagle, and Cenke Xu, “Classification and description of bosonic symmetry protected topological phases with semiclassical nonlinear sigma models,” *Phys. Rev. B* **91**, 134404 (2015).
  - <sup>18</sup> Zhen Bi and Cenke Xu, “Construction and field theory of bosonic-symmetry-protected topological states beyond group cohomology,” *Phys. Rev. B* **91**, 184404 (2015).
  - <sup>19</sup> Michael Hermele and Xie Chen, “Flux-Fusion Anomaly Test and Bosonic Topological Crystalline Insulators,” *Phys. Rev. X* **6**, 041006 (2016).
  - <sup>20</sup> Scott D. Geraedts and Olexei I. Motrunich, “Model Realization and Numerical Studies of a Three-Dimensional Bosonic Topological Insulator and Symmetry-Enriched Topological Phases,” *Phys. Rev. X* **4**, 041049 (2014).
  - <sup>21</sup> Scott D Geraedts and Olexei I Motrunich, “Exact models for symmetry-protected topological phases in one dimension,” arXiv preprint arXiv:1410.1580 (2014).
  - <sup>22</sup> Peng Ye and Zheng-Cheng Gu, “Topological quantum field theory of three-dimensional bosonic abelian-symmetry-protected topological phases,” *Phys. Rev. B* **93**, 205157 (2016).
  - <sup>23</sup> Peng Ye and Zheng-Cheng Gu, “Vortex-line condensation in three dimensions: A physical mechanism for bosonic topological insulators,” *Phys. Rev. X* **5**, 021029 (2015).
  - <sup>24</sup> Peng Ye and Xiao-Gang Wen, “Projective construction

- of two-dimensional symmetry-protected topological phases with  $U(1)$ ,  $SO(3)$ , or  $SU(2)$  symmetries,” *Phys. Rev. B* **87**, 195128 (2013).
- <sup>25</sup> Peng Ye and Xiao-Gang Wen, “Constructing symmetric topological phases of bosons in three dimensions via fermionic projective construction and dyon condensation,” *Phys. Rev. B* **89**, 045127 (2014).
- <sup>26</sup> M Zahid Hasan and Charles L Kane, “Colloquium: topological insulators,” *Reviews of Modern Physics* **82**, 3045 (2010).
- <sup>27</sup> Xiao-Liang Qi and Shou-Cheng Zhang, “Topological insulators and superconductors,” *Reviews of Modern Physics* **83**, 1057 (2011).
- <sup>28</sup> F.D.M. Haldane, “Continuum dynamics of the 1-D Heisenberg antiferromagnet: Identification with the  $O(3)$  nonlinear sigma model,” *Physics Letters A* **93**, 464–468 (1983).
- <sup>29</sup> Chong Wang, Adam Nahum, and T. Senthil, “Topological paramagnetism in frustrated spin-1 Mott insulators,” *Phys. Rev. B* **91**, 195131 (2015).
- <sup>30</sup> Juan Chamorro and Tyrel McQueen, “ $S = 1$  on a Diamond Lattice in  $\text{NiRh}_2\text{O}_4$ ,” APS March Meeting Abstract **B48.00006** (2017).
- <sup>31</sup> ee Supplemental Material at [url] for the detailed discussion.
- <sup>32</sup> Sumiko Horiuti and Syhei Miyahara, “Tetragonal Distortion of  $\text{NiRh}_2\text{O}_4$ ,” *Journal of the Physical Society of Japan* **19**, 423–424 (1964).
- <sup>33</sup> J.R. Chamorro and T.M. McQueen, “Frustrated  $S=1$  On A Diamond Lattice,” arXiv preprint arXiv:1701.06674 (2017).
- <sup>34</sup> Doron Bergman, Jason Alicea, Emanuel Gull, Simon Trebst, and Leon Balents, “Order-by-disorder and spiral spin-liquid in frustrated diamond-lattice antiferromagnets,” *Nature Physics* **3**, 487–491 (2007).
- <sup>35</sup> Shang Gao, Oksana Zaharko, Vladimir Tsurkan, Yixi Su, Jonathan S White, Gregory S Tucker, Bertrand Roessli, Frederic Bourdarot, Romain Sibille, Dmitry Chernyshov, *et al.*, “Spiral spin-liquid and the emergence of a vortex-like state in  $\text{MnSc}_2\text{S}_4$ ,” *Nature Physics* (2016).
- <sup>36</sup> SungBin Lee and Leon Balents, “Theory of the ordered phase in  $a$ -site antiferromagnetic spinels,” *Phys. Rev. B* **78**, 144417 (2008).
- <sup>37</sup> Lucile Savary, Emanuel Gull, Simon Trebst, Jason Alicea, Doron Bergman, and Leon Balents, “Impurity effects in highly frustrated diamond-lattice antiferromagnets,” *Phys. Rev. B* **84**, 064438 (2011).
- <sup>38</sup> Jean-Sébastien Bernier, Michael J. Lawler, and Yong Baek Kim, “Quantum order by disorder in frustrated diamond lattice antiferromagnets,” *Phys. Rev. Lett.* **101**, 047201 (2008).
- <sup>39</sup> Gang Chen, Michael Hermele, and Leo Radzihovsky, “Frustrated Quantum Critical Theory of Putative Spin-Liquid Phenomenology in  $6H\text{-B-Ba}_3\text{NiSb}_2\text{O}_9$ ,” *Phys. Rev. Lett.* **109**, 016402 (2012).
- <sup>40</sup> Matthew P. A. Fisher, Peter B. Weichman, G. Grinstein, and Daniel S. Fisher, “Boson localization and the superfluid-insulator transition,” *Phys. Rev. B* **40**, 546–570 (1989).
- <sup>41</sup> Tigran A. Sedrakyan, Leonid I. Glazman, and Alex Kamenev, “Absence of bose condensation on lattices with moat bands,” *Phys. Rev. B* **89**, 201112 (2014).
- <sup>42</sup> Tigran A. Sedrakyan, Leonid I. Glazman, and Alex Kamenev, “Spontaneous formation of a nonuniform chiral spin liquid in a moat-band lattice,” *Phys. Rev. Lett.* **114**, 037203 (2015).
- <sup>43</sup> Jan Attig and Simon Trebst, “Classical spin spirals in frustrated magnets from free-fermion band topology,” arXiv preprint arXiv:1705.04073 (2017).
- <sup>44</sup> Finn Lasse Buessen, Max Hering, Johannes Reuther, and Simon Trebst, “Quantum spin liquids in frustrated spin-1 diamond antiferromagnets,” arXiv preprint arXiv:1706.06299 (2017).
- <sup>45</sup> John B. Goodenough, “Spin-orbit-coupling effects in transition-metal compounds,” *Phys. Rev.* **171**, 466–479 (1968).
- <sup>46</sup> William Witczak-Krempa, Gang Chen, Yong Baek Kim, and Leon Balents, “Correlated Quantum Phenomena in the Strong Spin-Orbit Regime,” *Annual Review of Condensed Matter Physics* **5**, 57–82 (2014).
- <sup>47</sup> K.I. Kugel and D.I. Khomskii, *Sov. Phys. Usp.* **25**, 231 (1982).

# Supplementary Information for “Quantum Paramagnet and Frustrated Quantum Criticality in a Spin-One Diamond Lattice Antiferromagnet”

- I. Energy level of orbitals
- II. The magnetic susceptibility.
- III. Weiss mean-field theory in the quantum paramagnetic phase.
- IV. Exchange matrix.
- V. Quantum order by disorder.

## I. ENERGY LEVEL OF ORBITALS

In the main text, we assume that the degenerate  $xz$  and  $yz$  orbitals are above the  $xy$  orbital such that the orbital degree of freedom is fully quenched and we obtain the spin-only local moment with  $S = 1$  for the  $\text{Ni}^{2+}$  ion. Therefore, the atomic spin-orbit coupling is quenched at the linear order, and we can ignore the effect of the spin-orbit coupling if the crystal field splitting within the  $t_{2g}$  shell is larger than the spin-orbit coupling<sup>45</sup>. Under the above circumstances, the spin model in the main text is applicable to  $\text{NiRh}_2\text{O}_4$ .

If the degenerate  $xz$  and  $yz$  orbitals are below the  $xy$  orbital, there are two different electron filling schemes for the eight electrons in the  $\text{Ni}^{2+}$  ion (see Fig. 5). This degenerate filling arises from the degeneracy of the  $xz$  and  $yz$  orbitals. In this scenario, a pseudospin-1/2 degree of freedom would be introduced to describe the two-fold orbital degeneracy. Since the  $xz$  and  $yz$  orbitals belong to the  $t_{2g}$  orbital, the atomic spin-orbit coupling is active at the linear order<sup>46</sup>. Due to the orbital degree of freedom, the exchange interaction would be a Kugel-Khomskii superexchange interaction<sup>47</sup>. The potential interplay between the *on-site atomic spin-orbit coupling* and the *inter-site Kugel-Khomskii superexchange interaction* will be discussed in the future work.

It is not quite obvious right now whether the energy level scheme in the main text or in Fig. 5 applies to  $\text{NiRh}_2\text{O}_4$ . To resolve them, it would be nice to carry out an optical measurement to detect the energy level scheme of the  $\text{Ni}^{2+}$  ion. The existing experiment in Ref. 33 used  $\text{ZnRh}_2\text{O}_4$  to subtract the phonon contribution to the specific heat for  $\text{NiRh}_2\text{O}_4$  and found the magnetic entropy exceeds the spin-only contribution.  $\text{NiRh}_2\text{O}_4$  experiences a structural transition at 380K, and it is not obvious whether  $\text{ZnRh}_2\text{O}_4$  has the same structure as  $\text{NiRh}_2\text{O}_4$ . So using  $\text{ZnRh}_2\text{O}_4$  as the phonon background may be debatable.

## II. THE MAGNETIC SUSCEPTIBILITY

The presence of the single-ion anisotropy modifies the Curie-Weiss temperature. Since  $D_z > 0$  corresponds to the easy-plane spin anisotropy and tends to orient the

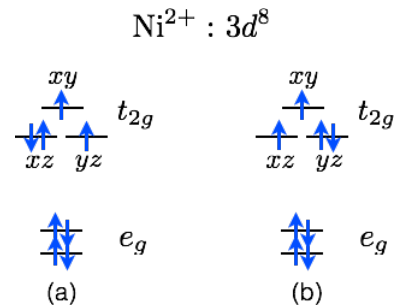


FIG. 5. (Color online.) The energy level diagram when the  $xz$  and  $yz$  orbitals are lower than the  $xy$  orbital. (a) and (b) are two equivalent electron filling schemes and can be represented by a pseudospin-1/2 orbital degree of freedom. See the text for the detailed discussion.

spin in the  $xy$  plane, so we expect  $D_z$  to contribute an antiferromagnetic (ferromagnetic) Curie-Weiss temperature when the external field is applied along the  $z$  direction (in the  $xy$  plane). To examine this, here we carry out the high temperature expansion and extract the Curie-Weiss temperature. In a magnetic field that is applied along the  $z$  direction, the Hamiltonian is

$$H_h = \sum_{\mathbf{r}, \mathbf{r}'} J_{\mathbf{r}\mathbf{r}'} \mathbf{S}_{\mathbf{r}} \cdot \mathbf{S}_{\mathbf{r}'} + \sum_{\mathbf{r}} [D_z (S_{\mathbf{r}}^z)^2 - h S_{\mathbf{r}}^z]. \quad (15)$$

The magnetization  $M^z$  is then given as

$$M^z = \sum_{\mathbf{r}} \frac{\text{Tr}[S_{\mathbf{r}}^z e^{-\beta H_h}]}{\text{Tr}[e^{-\beta H_h}]}, \quad (16)$$

from which one can carry out the expansion in  $\beta = 1/(k_B T)$ . The linear order in  $\beta$  is the free ion contribution without the single-ion anisotropy  $D_z$ . For the second order terms in  $\beta$ , besides the usual contribution from the crossing term between the superexchange and the Zeeman coupling, we now have a new contribution from the crossing term between the single-ion anisotropy and the Zeeman coupling. These crossing terms make non-vanishing contributions to the magnetization. From the magnetization, it is straightforward to read the susceptibility and the Curie-Weiss temperature. Likewise, the magnetization and the Curie-Weiss temperature for the field in the  $xy$  plane can also be obtained.

### III. WEISS MEAN-FIELD THEORY IN THE QUANTUM PARAMAGNET

Here we explain the zero-temperature spin susceptibility in the quantum paramagnet. From a general symmetry point of view, the global U(1) spin rotational symmetry around the  $z$  direction is preserved in the quantum paramagnet, so the total  $S^z$  is a good quantum number and we can use the total  $S^z$  to label all the states. The quantum paramagnet is a *gapped* spin singlet state with  $\sum_{\mathbf{r}} S_{\mathbf{r}}^z = 0$ . Thus it is obvious that the spin susceptibility for field applied along  $z$  direction is zero.

For the magnetic field in the  $xy$  plane, the system no longer has a global U(1) symmetry, and the above argument fails. To calculate the zero-temperature spin susceptibility, we take a Weiss mean-field approach and replace the spin model with a mean-field model, *i.e.*,

$$H_x = \sum_{\mathbf{r}\mathbf{r}'} J_{\mathbf{r}\mathbf{r}'} \mathbf{S}_{\mathbf{r}} \cdot \mathbf{S}_{\mathbf{r}'} + \sum_{\mathbf{r}} [D_z (S_{\mathbf{r}}^z)^2 - h_x S_{\mathbf{r}}^x] \quad (17)$$

$$\Downarrow$$

$$H_{\text{MFx}} = \sum_{\mathbf{r}\mathbf{r}'} J_{\mathbf{r}\mathbf{r}'} S_{\mathbf{r}}^x \langle S_{\mathbf{r}'}^x \rangle + \sum_{\mathbf{r}} [D_z (S_{\mathbf{r}}^z)^2 - h_x S_{\mathbf{r}}^x] \quad (18)$$

where  $\langle S_{\mathbf{r}}^x \rangle \equiv m^x$  and we assume a uniform mean-field ansatz. We solve for  $m^x$  self-consistently and obtain the magnetization,

$$m^x = \frac{2h_x}{D_z + 2(z_1 J_1 + z_2 J_2)} \quad (19)$$

and the spin susceptibility

$$\chi_{\perp} = \frac{2\mu_0 (g\mu_{\text{B}})^2}{D_z + 2(z_1 J_1 + z_2 J_2)}, \quad (20)$$

where we have put back in the physical units.

### IV. EXCHANGE MATRIX

The exchange matrix, that was introduced in the main text, is simply obtained by Fourier transform of the exchange part of the Hamiltonian. We have

$$\mathcal{J}_{\mathbf{k}} = \begin{bmatrix} J_2 \sum_{\mu=1}^{12} e^{i\mathbf{k}\cdot\mathbf{b}_{\mu}} & J_1 \sum_{\mu=1}^4 e^{i\mathbf{k}\cdot\mathbf{a}_{\mu}} \\ J_1 \sum_{\mu=1}^4 e^{-i\mathbf{k}\cdot\mathbf{a}_{\mu}} & J_2 \sum_{\mu=1}^{12} e^{i\mathbf{k}\cdot\mathbf{b}_{\mu}} \end{bmatrix}, \quad (21)$$

where  $\mathbf{a}_{\mu}$  are the four first neighbor vectors and  $\mathbf{b}_{\mu}$  are the twelve second neighbor vectors.

The eigenvalues of  $\mathcal{J}_{\mathbf{k}}$  are easily obtained

$$\xi_{1,\mathbf{k}} = 4J_2\alpha_{\mathbf{k}} + 2J_1(1 + \alpha_{\mathbf{k}})^{1/2}, \quad (22)$$

$$\xi_{2,\mathbf{k}} = 4J_2\alpha_{\mathbf{k}} - 2J_1(1 + \alpha_{\mathbf{k}})^{1/2}, \quad (23)$$

where

$$\alpha_{\mathbf{k}} = \cos \frac{k_x}{2} \cos \frac{k_y}{2} + \cos \frac{k_x}{2} \cos \frac{k_y}{2} + \cos \frac{k_x}{2} \cos \frac{k_y}{2}. \quad (24)$$

### V. QUANTUM ORDER BY DISORDER

In the ordered regime, the system develops a spin spiral order in the  $xy$  plane, and the mean-field theory for the ordered state yields the mean-field Hamiltonian for the  $xy$  spin components,

$$H_{xy} = \frac{1}{2} \sum_{\mathbf{q}} \sum_{i,j} \mathcal{J}_{\mathbf{q},ij} (S_{i,\mathbf{q}}^x S_{j,-\mathbf{q}}^x + S_{i,\mathbf{q}}^y S_{j,-\mathbf{q}}^y). \quad (25)$$

The ordering wavevector  $\mathbf{q}$  and the phase shift  $\theta_{\mathbf{q}}$  are determined by optimizing the eigenvalue and corresponding eigenvector of the exchange matrix. The optimal  $\mathbf{q}$  satisfies Eq.11 in the main text and forms a degenerate surface when  $J_2 > J_1/8$ , and this result is identical to the early classical treatment in Ref. 34. For the spin spiral state that is defined in Eq.13 and Eq.14 of the main text, the combined operation of the lattice translation and spin rotation around the  $z$  axis by the spiral angle remains to be a symmetry. We thus introduce the following Holstein-Primakoff boson for the spin spiral state,

$$\mathbf{S}_{\mathbf{r}} \cdot \hat{n}_{\mathbf{r}} = S - a_{\mathbf{r}}^{\dagger} a_{\mathbf{r}}, \quad (26)$$

$$\mathbf{S}_{\mathbf{r}} \cdot \hat{z} = \frac{\sqrt{2S}}{2} (a_{\mathbf{r}} + a_{\mathbf{r}}^{\dagger}), \quad (27)$$

$$\mathbf{S}_{\mathbf{r}} \cdot (\hat{n}_{\mathbf{r}} \times \hat{z}) = \frac{\sqrt{2S}}{2i} (a_{\mathbf{r}} - a_{\mathbf{r}}^{\dagger}), \quad (28)$$

where  $\hat{n}_{\mathbf{r}}$  is the orientation of the spin spiral order at the lattice site  $\mathbf{r}$ . With this substitution of the spin operators, we obtain the linear spin-wave Hamiltonian that is given as

$$H_{\text{sw}} = \sum_{\mathbf{k} \in \text{BZ}} (a_{1\mathbf{k}}^{\dagger}, a_{2\mathbf{k}}^{\dagger}, a_{1,-\mathbf{k}}, a_{2,-\mathbf{k}}) \times \begin{bmatrix} A_{\mathbf{k},11} & A_{\mathbf{k},12} & B_{\mathbf{k},11} & B_{\mathbf{k},12} \\ A_{\mathbf{k},12}^* & A_{\mathbf{k},22} & B_{-\mathbf{k},12} & B_{\mathbf{k},22} \\ B_{\mathbf{k},11}^* & B_{-\mathbf{k},12}^* & A_{-\mathbf{k},11} & A_{-\mathbf{k},12}^* \\ B_{\mathbf{k},12}^* & B_{\mathbf{k},22}^* & A_{-\mathbf{k},12} & A_{-\mathbf{k},22} \end{bmatrix} \begin{pmatrix} a_{1,\mathbf{k}} \\ a_{2,\mathbf{k}} \\ a_{1,-\mathbf{k}}^{\dagger} \\ a_{2,-\mathbf{k}}^{\dagger} \end{pmatrix} - \sum_{\mathbf{k} \in \text{BZ}} (A_{\mathbf{k},11} + A_{\mathbf{k},22}), \quad (29)$$

where

$$A_{\mathbf{k},11} = A_{\mathbf{k},22} = \frac{D_z}{2} - \frac{J_1}{2} \sum_{\mu=1}^4 \cos(\mathbf{q} \cdot \mathbf{a}_{\mu} + \theta_{\mathbf{q}}) + \frac{J_2}{4} \sum_{\mu=1}^{12} [\cos(\mathbf{k} \cdot \mathbf{b}_{\mu}) + (\cos(\mathbf{k} \cdot \mathbf{b}_{\mu}) - 2) \cos(\mathbf{q} \cdot \mathbf{b}_{\mu})], \quad (30)$$

$$A_{\mathbf{k},12} = \frac{J_1}{4} \sum_{\mu=1}^4 e^{i\mathbf{k}\cdot\mathbf{a}_{\mu}} [1 + \cos(\mathbf{q} \cdot \mathbf{a}_{\mu} + \theta_{\mathbf{q}})], \quad (31)$$

$$B_{\mathbf{k},11} = \frac{D_z}{2} + \frac{J_2}{4} \sum_{\mu=1}^{12} \cos(\mathbf{k} \cdot \mathbf{b}_{\mu}) [1 - \cos(\mathbf{q} \cdot \mathbf{b}_{\mu})], \quad (32)$$

$$B_{\mathbf{k},12} = \frac{J_1}{8} \sum_{\mu=1}^4 \cos(\mathbf{k} \cdot \mathbf{a}_{\mu}) [1 - \cos(\mathbf{q} \cdot \mathbf{a}_{\mu} + \theta_{\mathbf{q}})], \quad (33)$$

and  $a_{1,\mathbf{k}}$  and  $a_{2,\mathbf{k}}$  represent the Holstein-Primakoff boson on the A and the B sublattices, respectively.

The spin-wave Hamiltonian is diagonalized by a Bogoliubov transformation. The quantum zero point energy is given as

$$\Delta E = \sum_{\mathbf{k}} \sum_{i=1}^2 \frac{1}{2} \Omega_{\mathbf{k},i} - \sum_{\mathbf{k}} 2A_{\mathbf{k},11}, \quad (34)$$

where  $\Omega_{\mathbf{k},i}$  is the  $i$ -th spin-wave mode at the momentum  $\mathbf{k}$ .

In the phase diagram in Fig.2 of the main text, the

propagating wavevectors of the [111] spin spiral and the [001] spin spiral are uniquely specified by the intersection between the orientation and the degenerate surface. Here we describe the [111\*] spin spirals. As we have already pointed out in the main text, for  $J_2 > J_1/4$ , there is no intersection between the 111 axis and the degenerate surface. Instead, the Brillouin zone boundary/surface, that is normal to the 111 axis, intersects with the degenerate surface, and the interaction is a deformed circle (see Fig.4b). The quantum fluctuation selects the propagating wavevector on this deformed circle. Due to the cubic symmetry, six equivalent wavevectors on the deformed circle are selected.